Injection energy dependence of spin-polarized hot-electron transport through a ferromagnetic metal/oxide/semiconductor junction

N. Rougemaille,* D. Lamine, G. Lampel, Y. Lassailly, and J. Peretti†
Physique de la Matière Condensée, Ecole Polytechnique, CNRS, 91128 Palaiseau, France
(Received 8 October 2007; revised manuscript received 3 January 2008; published 12 March 2008)

Spin-polarized hot electron transport through a ferromagnetic metal/oxide/semiconductor junction is studied as a function of the electron injection energy in the range from a few eV up to 1 keV. The incident spin-polarized electrons are produced by a GaAs photocathode and are injected from vacuum into the thin metal layer. The current transmitted through the junction is measured in the semiconductor collector. A spin-dependent component of the transmitted current is detected when reversing either the spin polarization of the incident electrons or the magnetization of the metal layer. For injection energy in the hundreds of eV range, both the mean transmitted current and the spin-dependent transmitted current exhibit a spectacular increase, over several orders of magnitude. A transport regime is reached where electron transmission is larger than unity, providing a current gain, while the spin selectivity of the magnetic layer is still very high (close to 100%). This variation is analyzed in the framework of a transport model which accounts for the relaxation of the electron energy and velocity by secondary electron excitation. This model fits with the experimental data and evidences the crucial role of the metal/oxide/semiconductor barrier shape on the spin-dependent transport properties of the device.

DOI: 10.1103/PhysRevB.77.094409 PACS number(s): 72.25.−b, 73.40.Qv, 79.20.Hx, 85.75.−d

I. INTRODUCTION

In ferromagnetic metals, because of the spin asymmetry of the electron density of empty states, the inelastic mean free path is larger for majority-spin electrons than for minority-spin electrons in an energy range which extends up to about 50 eV above the Fermi Level. This favors the transport of majority-spin hot electrons and is at the origin of electron spin filtering effects in thin magnetic films.[1–8] Different experimental approaches have been developed to explore spin-dependent hot-electron transport in thin magnetic films. They are based either on electron spectroscopy techniques[5–14] or on three-terminal solid state devices,[15–21] and give access to the transport properties in a wide energy range, typically between 1 eV up to several hundreds of eV. The principle of all these experiments is basically the same: hot electrons are injected into a thin magnetic film and the intensity (or polarization) of the current transmitted through the film is detected. The transmitted current exhibits a spin asymmetry which is measured by reversing the incident electron polarization and/or the magnetization state of the film.

The largest values of hot-electron transmission spin asymmetry through thin ferromagnetic films are obtained at low injection energy, i.e., a few eV above the metal Fermi level.[9,10,12,14–21] In this energy range, the electron transmission through the thin magnetic layer is almost ballistic and is described by an exponential attenuation with the mean free path as relevant attenuation length. From the spin asymmetry of the mean free path, one can define a spin-discriminating length which is found to be as small as a few nanometers (typically 3–5 nm) for electrons of a few eV energy.[14,18] A magnetic layer of thickness of the order of the spin discriminating length is therefore highly spin selective. Spin-filtering efficiency close to unity has indeed been demonstrated in magnetic layers of only a few nanometers thickness. However, operating a spin filter at low injection energy is limited by the low total transmission efficiency. The mean transmitted current is indeed generally orders of magnitude smaller than the injected current mainly because of the weak exit probability of low energy electrons from the metal.[15–21]

At higher injection energy, the situation is very different. The contribution of ballistic transport is negligible and the transmitted current is dominated by electrons which emerge from a secondary electron cascade at energy much smaller than the injection energy. Therefore, the transport is governed by the electronic properties over a wide energy range. When the injection energy ranges from a few eV to several tens of eV, the electron inelastic mean free path stiffly decreases so that electrons are very efficiently relaxed. The transport can then be simply described as a two-step process: the formation of the secondary electron cascade in the very first atomic layer and the subsequent low-energy ballistic transport through the magnetic film.[9,10,12,14,18] This scheme has two consequences: the overall transmitted current increases with injection energy because of the secondary electron multiplication and the magnetic layer spin selectivity is still high because the electrons cross most of the distance through the metal layer with a low energy. One can profit from these two properties in spin-valve structures. Indeed, in a spin-valve structure containing only two magnetic layers (of about 1 nm thickness each), large magnetocurrent asymmetry has been obtained in the whole injection energy range from a few eV up to 100 eV, while the secondary electron multiplication yielded a linear increase in the transmitted current with injection energy.[14] Similar experiments performed in a single magnetic layer structure have shown that the transmission asymmetry measured when injecting spin-polarized electrons decreases inversely to the increase in the total transmitted current with injection energy.[9,10,12,18] This result is not contradictory with the spin-valve experiment. Indeed, the magnetic layer is still spin selective but the incident electron polarization is "diluted" by the secondary elec-

trons before the spin filter operates. In other words, when spin-polarized incident electrons are injected into a metallic film containing a single magnetic layer, the secondary electrons do not contribute to the spin-dependent transmitted current which all originates from the spin filtering of the only primary electrons. This is an important result as it means that the polarization of secondary electrons does not depend on the one of the injected electrons and that the effect of exchange integral asymmetry on the secondary electron polarization is negligible. For injection energies higher than 100 eV, the extension of the transport scheme mentioned above does not predict any particular behavior. However, the situation is again very different, in particular, because of the increase in the electron mean free path, and electron transmission experiments at injection energies of several hundreds of eV exhibits strong deviations from the simple transport model which fits at moderate injection energy.[22]

In the present paper, we report on a study of spin-polarized electron transport through a ferromagnetic metal/oxide/semiconductor junction, where the electron injection energy is varied from a few eV up to 1 keV. The experimental configuration can be compared to a three-terminal device geometry,[15–21] the emitter being here a GaAs spin-polarized electron source separated from the metallic base by vacuum. This allows an easy control of the electron injection energy and of the polarization. At moderate injection energy (from 8 to 100 eV above the metal Fermi level), results are similar to the one obtained in previous studies.[9,12,14,18] However, above 100 eV injection energy, the increase in the transmitted current becomes superlinear and the spin-dependent transmitted current rises by several orders of magnitude, increasing even faster than the transmitted current. This feature clearly differs from what could be predicted from any previous studies performed at moderate injection energy. We have developed a model to describe the transport of spin-polarized hot electron through the metal/oxide/semiconductor structure. Qualitative and quantitative agreement with the experimental data is obtained over the whole probed injection energy range. This model is based on the calculation of the electron energy distribution that results from the secondary electron cascade in the metallic layer and of the electron transfer into the semiconductor collector through the junction barrier. Both the energy and velocity relaxation of the incident electrons, by excitation of secondary electrons from the metal Fermi sea, are taken into account. The data analysis in the framework of this model shows that the increase in the electron transmission and in the spin-dependent transmission, observed when the injection energy exceeds several hundreds of eV, is a combined effect of the broadening of the electron energy distribution and of the variation with energy of the electron transfer efficiency at the base-collector junction. It turns out that a hot-electron spin-filtering device that has a controlled barrier shape at the base-collector interface and that can be operated at injection energy of several hundreds of eV exhibits striking transport regimes. In particular, a structure having a thin oxide interfacial layer between the magnetic metal base and the semiconductor collector combines high spin selectivity (close to unity) and high electron transmission (larger than unity), opening up the possibility to achieve large magnetocurrent asymmetry together with current gain. For other specific base-collector barrier shape, a sign reversal of the transmission spin asymmetry could even be obtained at high injection energy due to the spin dependence of the secondary electron multiplication efficiency in the magnetic layer.

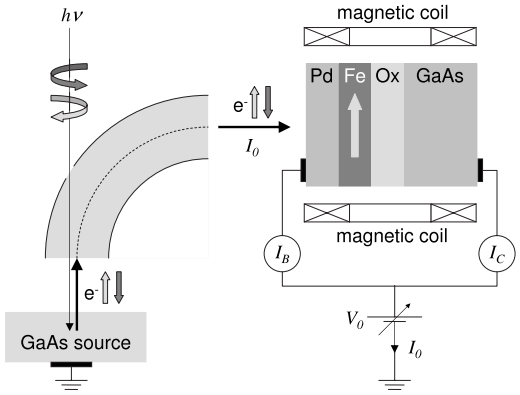

FIG. 1. Schematic of the experimental setup and principle.

II. EXPERIMENT

The spin-polarized electron transmission experiment is performed in a UHV chamber with a base pressure of a few 10^{-11} Torr. The principle of this experiment is schematized in Fig. 1.

The sample is a Pd/Fe/oxide/GaAs junction. The semiconductor collector is a 1-μm-thick n-doped (10^{16} cm^{-3}) GaAs layer grown on an n^+-doped (001) GaAs substrate with an Ohmic back contact. A 2-nm-thick oxide layer is formed on the surface of the GaAs top layer by exposure to UV light and ozone. This thin oxide layer avoids interdiffusion between the GaAs and the subsequently grown metallic film and contributes to the junction potential barrier.[23] The metallic film is made of a Fe layer, of thickness $d_{\mathrm{Fe}}=3.5$ nm, covered by a Pd cap layer, of thickness $d_{\mathrm{Pd}}=5$ nm, which prevents the iron from oxidation. The Fe layer exhibits an in-plane magnetization square hysteresis loop, with a coercive field of about 50 Oe and a remanent magnetization m_R close to the saturation magnetization m_S ($m_R=0.9m_S$). This allows us to reverse the Fe layer magnetization from $+m_R$ to $-m_R$ by pulsed-current operation of an *in situ* magnetic coils and to measure the spin-dependent transmitted current at zero external magnetic field.

The spin-polarized electron beam is produced by a GaAs photocathode activated to negative electron affinity by cesium and oxygen deposition. Under excitation with a circularly polarized near-band gap laser light (of energy $h\nu=1.58$ eV), this source yields an electron beam of longitudinal spin polarization P_0, which can be switched between +25% and −25% by reversing the light polarization. This electron beam passes through a cylindrical electrostatic deflector to convert the longitudinal spin polarization into a transverse one aligned along the Fe-layer magnetization axis. The beam is then focused onto the sample by electrostatic electron optics. The electron injection energy E_0, referred to the metal Fermi level, is controlled by the sample potential

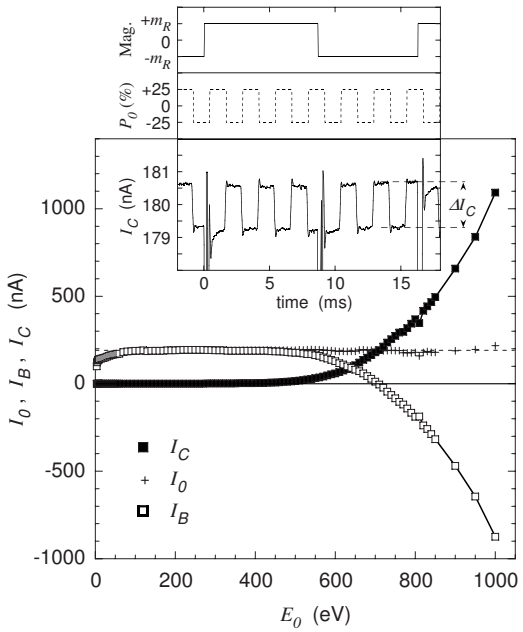

FIG. 2. Variation, with the injection energy E_0, of the injection current I_0, of the base current I_B, and of the transmitted current I_C. In the inset is shown the collected current change due to the spin-dependent electron transmission. For this measurement, the energy was set at $E_0=712$ eV and the incident electron polarization was modulated between +25% and −25% at a frequency of 400 Hz. The magnetization of the Fe layer was several times flipped during the measurement by pulsed current operation of the magnetic coil. The configurations $[+m_R,+P_0]$ and $[-m_R,-P_0]$ give the same value I_C^+ of the collector current, while the configurations $[+m_R,-P_0]$ and $[-m_R,+P_0]$ give both the value I_C^-. This shows that instrumental asymmetries are negligible.

V_0. A typical incident current of 200 nA, with a 200 meV energy distribution width, is injected into the junction.

By analogy, with the three-terminal transistorlike devices, the currents flowing in the metallic layer ("base") and in the semiconductor ("collector") are labeled I_B and I_C, respectively. The injected current is labeled I_0. These three currents are independently measured using homemade isolated current amplifiers, which may operate at 1 kV with an electronic noise of 30 fA/$\sqrt{\text{Hz}}$. The independent measurement of I_0 is performed by disconnecting one of the two (base or collector) terminals, and then using the sample as a collecting anode. Figure 2 shows the experimental variation of I_0, I_B, and I_C with the injection energy E_0. The injected current I_0 is constant as soon as the sample potential is significantly larger than the potential of the last electrode of the electron optics (40 V). However, at low sample potential, the injection efficiency is at most reduced by 40%. The current conservation relation $I_0=I_B+I_C$ is experimentally verified over the whole probed energy range. This indicates that the electron injection setup is properly shielded, allowing reliable measurements of very weak transmitted current. At low injection energy, the base current I_B is almost equal to I_0 since the transmitted current I_C is very small. However, at high injection energy, I_C strongly increases and becomes larger than the injected current I_0 above $E_0=712$ eV. At the same time, the base current I_B decreases, drops down to zero at $E_0=712$ eV, and then becomes negative. Since I_C increases and overcomes the value of the injected current, it is clear that the transport through the metal is mainly governed by electron-electron scattering, providing electron multiplication by excitation of a secondary electron cascade.

The spin-dependent component of the transmitted current $\Delta I_C=I_C^+-I_C^-$ is the difference between the values I_C^+ and I_C^- of the collector current for an incident electron spin polarization of, respectively, $+P_0$ and $-P_0$. As an example, the measurement of ΔI_C, when the injection energy is set at 712 eV (the energy where $I_C=I_0$ and $I_B=0$), is shown in the inset of Fig. 2. For this measurement, the incident electron polarization was flipped between $+P_0$ and $-P_0$ by modulating the incident light polarization between σ^+ and σ^- at a frequency of 400 Hz. For each value of the injection energy, ΔI_C is systematically measured for the two opposite magnetizations $+m_R$ and $-m_R$ of the Fe layer. This allows us to get rid of instrumental asymmetries which are, however, very low in the present experiment. Indeed, as shown in the inset of Fig. 2, reversing the incident electron polarization or the sample magnetization produces the same transmitted current variation. This is what is expected in the absence of instrumental asymmetries since the spin-filtering effect only depends on the orientation of the incident electron polarization relative to that of the magnetization.

For the analysis of the experimental data, we will consider the three following dimensionless quantities:

(i) $T=I_C/I_0$, the transmission;

(ii) $\Delta T=\Delta I_C/I_0$, the spin dependent transmission; and

(iii) $A_C=(I_C^+-I_C^-)/(I_C^++I_C^-)=\Delta T/2T$, the transmission spin asymmetry.

Note that these three normalized quantities are not affected by the decrease in the injection efficiency at low sample potential. The variations of T and ΔT as a function of E_0 are plotted in Fig. 3(a). The transmission T varies over almost 6 orders of magnitude and clearly exhibits three regimes. In the low-energy range, up to about 80 eV, T increases linearly with E_0. In the intermediate energy range, between 80 and 350 eV, the increase in T is more pronounced. Finally, above 350 eV, T steps up abruptly and goes beyond unity. The variation of the spin dependent transmission ΔT also reveals three regimes in the same three energy ranges. At low injection energy, ΔT is constant as observed in all the previous similar experiments.[9,10,12,14,18] However, beyond 80 eV, the spin-dependent transmission increases over four orders of magnitude. In the high-energy range, the increase in ΔT is particularly spectacular as it is even faster than that of the transmission T. This is evidenced by the variation of the transmission spin asymmetry A_C [Fig. 3(b)] which exhibits a jump by an order of magnitude between 350 and 800 eV injection energies. This feature is a strong deviation from the constant decrease which was expected from the previous studies performed at moderate injection energy.

III. THEORETICAL MODEL

A. Overview of the model

In this section, we will first consider the case of an unpolarized electron beam injected in a nonmagnetic metal/oxide/

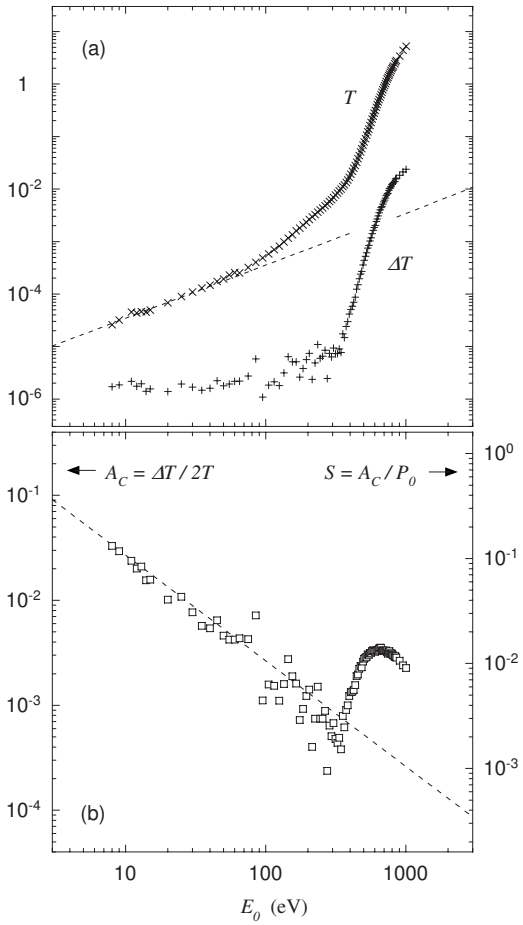

FIG. 3. (a) Variation of the transmission T ($\times$) and of the spin dependent transmission ΔT ($+$) with the injection energy E_0. The dashed line corresponds to a linear increase in E_0. (b) Variation of the transmission spin asymmetry A_C ($\square$) with the injection energy E_0. The dashed line corresponds to a decrease proportional to $1/E_0$. The right-hand vertical axis gives the corresponding value of $S = A_C/P_0$, the asymmetry for a 100% polarized incident beam. This quantity is analogous to the Sherman function in spin polarimetry.

semiconductor structure. We assume that the transport is governed by electron-electron scattering yielding a secondary electron cascade. This results in the formation of an electron distribution mixing primary and secondary electrons. The distribution $F(\varepsilon)$ that reaches the metal/oxide/semiconductor junction may be written as

$$F(\varepsilon) = Mf(\varepsilon), \tag{1}$$

where $f(\varepsilon)$ is the normalized distribution of electrons and M the multiplication factor related to the secondary electron cascade. Then, electrons are transferred through the junction barrier into the semiconductor collector with an efficiency $\alpha(\varepsilon)$. The transmitted electrons collected in the semiconductor form the current I_C. The electrons which cannot cross the barrier contribute to the base current I_B, together with the holes produced in the metal by the excitation of the secondary electrons. Following these ideas, the electron transmission T can be written as

$$T = M\int_0^{+\infty} \alpha(\varepsilon) f(\varepsilon) d\varepsilon. \tag{2}$$

At the metal/semiconductor interface, the collection efficiency $\alpha(\varepsilon)$ is known to be an increasing function of the collection energy ε above the barrier of the Schottky junction.[21] In the sample studied here, this tendency is reinforced by the presence of the oxide layer. Indeed, two barriers have to be considered: the semiconductor band bending barrier of height ϕ_{SC}=0.78 eV,[24] and the oxide layer barrier of height ϕ_{ox}=4.5 eV much larger than ϕ_{SC}.[24–26] We will therefore assume that $\alpha(\varepsilon)$ has a step shape.

(i) For $\varepsilon < \phi_{SC}$, the electron cannot be transmitted in the semiconductor and the barrier transfer efficiency $\alpha(\varepsilon)$ is zero.

(ii) For $\phi_{SC} < \varepsilon < \phi_{ox}$, the electrons may cross the oxide layer by a tunneling process or through defects and the transfer efficiency $\alpha(\varepsilon)$ takes a value α_{SC} very small when compared to unity.

(iii) For $\phi_{ox} < \varepsilon$, the electrons are transmitted above the oxide barrier and $\alpha(\varepsilon)$ takes a value α_{ox} much larger than α_{SC} the transfer efficiency below the oxide barrier.

If we assume that α_{SC} and α_{ox} are constant over the, respectively, relevant energy intervals, the expression of T becomes

$$T = T_{SC} + T_{ox} = M\left[\alpha_{SC}\int_{\phi_{SC}}^{\phi_{ox}} f(\varepsilon)d\varepsilon + \alpha_{ox}\int_{\phi_{ox}}^{+\infty} f(\varepsilon)d\varepsilon\right]. \tag{3}$$

When increasing the injection energy, it is clear that the secondary electron multiplication factor M increases but also that the electron distribution tends to broaden. Both contribute to the rise in T. For low injection energies, one can intuitively assume that $f(\varepsilon)$ remains narrow and, since ϕ_{SC} is much smaller than ϕ_{ox}, T is mainly given by the term T_{SC} and increases like M. At higher injection energy, because of the broadening of $f(\varepsilon)$ and since α_{ox} is much larger than α_{SC}, the term T_{ox} may become predominant and a more pronounced increase in T is expected. This picture is qualitatively in agreement with the experimental results as it predicts that the increase in T with injection energy features different regimes.

B. Calculation of the electron cascade

The calculation of the transmission T requires the explicit calculation of the electron energy distribution that results from the electron cascade. We assume that this distribution can be approximated by an exponential function,

$$f(\varepsilon) = \frac{1}{E_M}\exp\left(-\frac{\varepsilon}{E_M}\right). \tag{4}$$

The choice of an exponential shape does not mean that we are considering a thermalized electron distribution but aims at describing conveniently the accumulation of electrons at low energy that results from the secondary electron cascade. Note that the energy-resolved electron transmission experi-

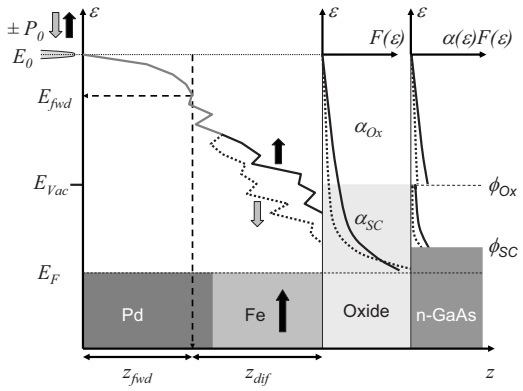

FIG. 4. Schematics of the electron relaxation process through the metal layer and of the transmission through the junction barrier. Incident electrons are injected into the Pd layer with a polarization $\pm P_0$ and an energy E_0 with respect to the metal Fermi level. They cross the distance z_{fwd} before their velocity is relaxed. At this point, their mean energy is E_{fwd}. Then they cross the remaining distance z_{dif} to the junction by a three-dimensional diffusionlike transport process. In the magnetic layer, the relaxation is different for majority and minority spin electrons leading to two different distributions at the junction. The current transmitted into the semiconductor collector is the sum of two contributions: the electrons transmitted above the semiconductor band-bending barrier ϕ_{SC} with the transfer efficiency α_{SC} and the electrons transmitted above the oxide barrier ϕ_{ox} with the transfer efficiency α_{ox} oxide.

ments through metallic membranes have shown that the transmitted electron distribution has indeed an exponential shape.[10] The calculation of the cascade then reduces to the determination of two quantities: the electron mean energy E_M, which characterizes the width of the electron distribution, and the secondary multiplication factor M, which gives the amplitude of the electron distribution.

To proceed with this calculation, we will take into account both energy and velocity relaxation by electron-electron scattering. A schematic of the electron cascading through the metallic layer is shown in Fig. 4. An incident electron enters the metallic layer at $z=0$ with an energy E_0 and a velocity $\vec{v}_0$ perpendicular to the metal surface (i.e., longitudinal). Along the transport through the metal layer, it relaxes its energy and velocity by exciting a secondary electron cascade. The electron distribution which forms along the transport through the metal layer has a mean energy ε and a mean velocity $\vec{v}$ of longitudinal component v_l. As long as v_l is larger than the Fermi velocity v_F, we consider that the electron velocity is not relaxed and that forward scattering is favored. The velocity relaxation is completed over a distance z_{fwd} (see Fig. 4). At this distance from the surface, the electron distribution has a mean energy that we note E_{fwd}. The longitudinal component of the electron velocity v_l then becomes smaller than v_F, and further collisions randomize the scattering direction. A diffusionlike regime takes place over a distance z_{dif} before the electron distribution reaches the metal/oxide interface with a mean energy E_M.

In the velocity-relaxation transport regime, i.e., for $0<z<z_{fwd}$, we consider that after each collision between an electron of energy ε and of longitudinal velocity component v_l, and an electron of the Fermi sea, two electrons emerge with a mean energy $\varepsilon/2$ and a mean longitudinal velocity component $v_l/2$. We here neglect the energy and momentum given to the hole left in the Fermi sea by the excitation of the secondary electron. The time evolution of the mean electron energy and of the mean longitudinal velocity component can then be written as two relaxation equations,

$$\frac{d\varepsilon}{dt} = -\ln 2 \frac{\varepsilon}{\tau}, \tag{5}$$

and

$$\frac{dv_l}{dt} = -\ln 2 \frac{v_l}{\tau}. \tag{6}$$

where τ the electron-electron collision time depends on energy. We can then write a propagation equation of the form

$$\frac{dz}{d\varepsilon} = \frac{dz}{dt}\frac{dt}{d\varepsilon} = -v_l \frac{1}{\ln 2}\frac{\tau}{\varepsilon}, \tag{7}$$

where v_l, the longitudinal component of the mean electron velocity, is obtained by combining Eqs. (5) and (6),

$$v_l = v_0 \frac{\varepsilon}{E_0}. \tag{8}$$

In a parabolic band approximation, the incident electron velocity modulus is given by

$$v_0 = v_F \sqrt{\frac{E_0 + E_F}{E_F}}, \tag{9}$$

where E_F is the Fermi energy (referred to the bottom of the parabolic band).

When the velocity is relaxed, the longitudinal component of the electron velocity is $v_l = v_F$ (which is the criterion chosen for the transition between the two transport regime) and the average electron energy is $\varepsilon = E_{fwd}$. We then obtain for the value of the mean electron energy at the distance z_{fwd} from the surface,

$$E_{fwd} = E_0 \sqrt{\frac{E_F}{E_0 + E_F}}. \tag{10}$$

The velocity relaxation path z_{fwd} is then obtained after integration of Eq. (7),

$$z_{fwd} = -\frac{1}{\ln 2}\int_{E_0}^{E_{fwd}} v_l \tau \frac{d\varepsilon}{\varepsilon} = \frac{1}{\ln 2}\int_{E_{fwd}}^{E_0} \lambda(\varepsilon) \sqrt{\frac{E_0 + E_F}{\varepsilon + E_F}} \frac{d\varepsilon}{E_0}, \tag{11}$$

where $\lambda(\varepsilon) = v\tau$ is the electron mean free path.

After crossing the distance z_{fwd}, we consider that the electron velocity is relaxed and that the scattering direction is randomized. A three-dimensional diffusionlike transport regime takes place which can be described by the evolution equation,

$$\frac{dz^2}{dt} = \frac{1}{3}D(\varepsilon), \tag{12}$$

where the quantity $D(\varepsilon)$ is similar to an energy-dependent diffusion coefficient and is given by

$$D(\varepsilon) = v^2\tau. \tag{13}$$

Along this transport regime, the mean energy of the electron distribution decreases from E_{fwd} to E_M according to the energy relaxation equation [Eq. (5)]. The propagation equation then becomes

$$\frac{dz^2}{d\varepsilon} = \frac{dz^2}{dt}\frac{dt}{d\varepsilon} = -\frac{1}{3}\frac{1}{\ln 2}\frac{v^2\tau^2}{\varepsilon}, \tag{14}$$

so that the distance crossed in the diffusion regime is given by

$$z_{dif}^2 = -\frac{1}{3\ln 2}\int_{E_{fwd}}^{E_M} \lambda^2(\varepsilon)\frac{d\varepsilon}{\varepsilon}. \tag{15}$$

For the calculation of z_{fwd} and z_{dif} after Eqs. (11) and (15), we have taken E_F=7 eV, which is close to the value of the Fermi energy in palladium, and we have used an empirical form for $\lambda(\varepsilon)$ (see Appendix A),

$$\lambda(\varepsilon) = \lambda_l\left(\frac{E_l}{\varepsilon + E_l}\right)^{a_l} + \lambda_h\left(\frac{\varepsilon}{\varepsilon + E_h}\right)^{a_h} - \lambda_{off}. \tag{16}$$

The electron mean energy E_M at the junction barrier which appears as an integration limit in Eq. (15) is then obtained by solving the equation

$$d = z_{fwd} + z_{dif}, \tag{17}$$

where d is the total thickness of the metallic base.

The resulting variation of E_M with injection energy E_0 is plotted in Fig. 5 together with the variation of the velocity-relaxation path z_{fwd}. In the low injection energy range, i.e., below 80 eV, z_{fwd} is very short (a few tenth of nanometer) and almost constant: the electron velocity is very quickly relaxed and the diffusionlike transport step takes place almost all over the metal layer thickness. The result is that E_M remains almost constant and takes a value, small when compared to both junction barriers ϕ_{SC} and ϕ_{ox}. In the high injection energy range, i.e., above typically 80 eV, z_{fwd} starts to rapidly increase and reaches a value of several nanometer at 1000 eV, which is a significant part of the total metal layer thickness. Velocity relaxation requires a longer path, so that the electrons penetrate more deeply into the metallic layer before the diffusive regime takes place. Therefore, energy relaxation is less efficient and E_M increases. It even reaches values larger than the semiconductor band bending ϕ_{SC}.

C. Calculation of T as a function of E_0

The average number n of collisions that an electron undergoes during the transport through the metal layer is given by

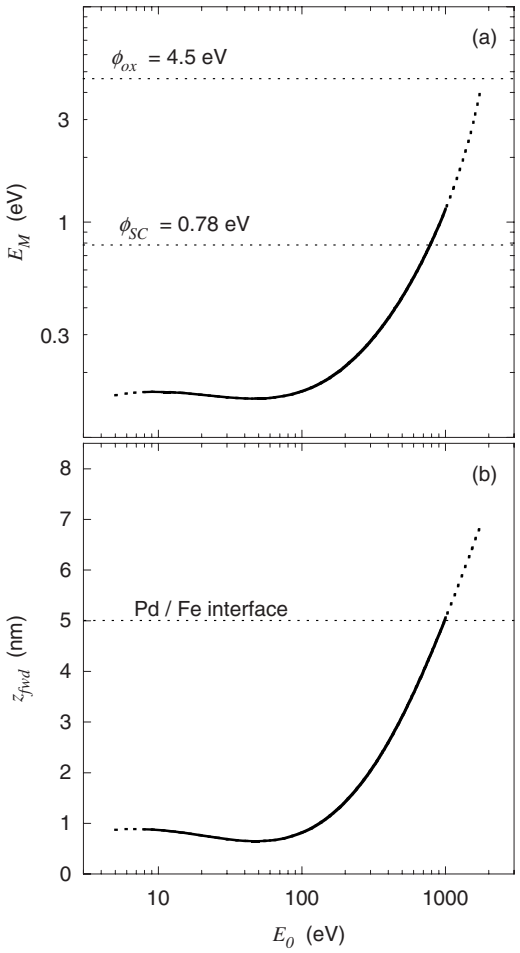

FIG. 5. (a) Calculated variation of the electron mean energy E_M at the metal/oxide interface as a function of the injection energy E_0. The horizontal dotted lines indicate the values of the two barrier heights ϕ_{SC} and ϕ_{ox}. (b) Calculated variation of the distance z_{fwd} crossed through the metal layer as a function of the injection energy E_0. The vertical scale corresponds to the total metal base thickness d=8.5 nm. The horizontal dotted line indicates the position of the Pd/Fe interface.

$$n = \int_0^{t_M} \frac{dt}{\tau}, \tag{18}$$

where t_M is the total time that takes the average electron to cross the metal layer. During this time, the average electron cascades from E_0, the injection energy, to E_M, the mean energy at the metal/oxide interface. According to Eq. (5), the average number of collisions during the transport is then given by

$$n = -\int_{E_0}^{E_M} \frac{1}{\ln 2}\frac{d\varepsilon}{\varepsilon} = \frac{1}{\ln 2}\ln\left(\frac{E_0}{E_M}\right). \tag{19}$$

Since each collision yields two electrons (the incoming electron and the secondary electron excited from the Fermi sea), the multiplication factor M is

$$M = 2^n = \frac{E_0}{E_M}. \quad (20)$$

The multiplication factor simply reflects the fact that the primary electron energy E_0 is shared with the M electrons (the primary and the secondaries) of mean energy E_M.

Combining Eqs. (3), (4), and (20) and assuming that $E_0 \gg E_M$ and $\alpha_{ox} \gg \alpha_{SC}$, we then obtain a simple expression for the transmission through the junction.

$$T \approx \frac{E_0}{E_M}\left[\alpha_{SC}\exp\left(-\frac{\phi_{SC}}{E_M}\right) + \alpha_{ox}\exp\left(-\frac{\phi_{ox}}{E_M}\right)\right]. \quad (21)$$

Using the variation of E_M with E_0 calculated in the previous section, we obtain the theoretical variation of the transmission T versus E_0 plotted in Fig. 6(a). For this calculation, we have used the values of the two barrier heights already mentioned: ϕ_{SC}=0.78 eV and ϕ_{ox}=4.5 eV, and we have taken for the transmission coefficients $\alpha_{SC}=10^{-4}$ and $\alpha_{ox}=0.5$ which are reasonable estimations of the transmission probability above ϕ_{SC} (through the oxide barrier) and above ϕ_{ox}, respectively. Details concerning the choice of the parameters and the fitting procedure are given in Appendix A.

The calculated variation of T reproduces the three regimes observed experimentally. In the first regime, the electron mean energy E_M remains almost constant, as shown in Fig. 5(a), and the linear increase in T with E_0 is due to the multiplication factor $M=E_0/E_M$. For injection energies larger than 80 eV, the second regime starts, characterized by a superlinear increase in T with E_0. As previously mentioned, when increasing E_0 the velocity-relaxation path z_{fwd} increases (due to the increase in both the injected electron velocity and the electron mean free path), which causes an increase in the electron distribution mean energy E_M at the metal/oxide interface. Thus, a larger number of electrons may overcome the barrier and be transmitted in the semiconductor. In the third regime, above 350 eV injection energy, the electron mean energy has so increased that the transmission is dominated by electrons of energy higher than the oxide barrier height ϕ_{ox}. The two contributions to the transmission above ϕ_{SC}, through the oxide barrier, and above ϕ_{ox} are plotted separately in Fig. 6(a) (dotted and dashed lines). It is clear that with the increase in E_M, the transmission goes from a regime dominated by electrons of energy just larger than ϕ_{SC} (despite the fact that α_{SC} is very small when compared to α_{ox}) to a regime dominated by electrons of energy larger than ϕ_{ox}.

D. Calculation of ΔT and A_C as a function of E_0

The electronic distribution $F(\varepsilon)$ that forms during the transport through the metallic layer mixes primary and secondary electrons. Because of the spin dependence of the electron mean free path in a magnetic metal layer, we will consider separately three electron distributions: the primary electron distribution with spin parallel to the majority spin, the primary electron distribution with spin parallel to the minority spin, and the secondary electron distribution. We may somehow "distinguish" between primary and secondary electrons because primaries are spin tagged and we assume

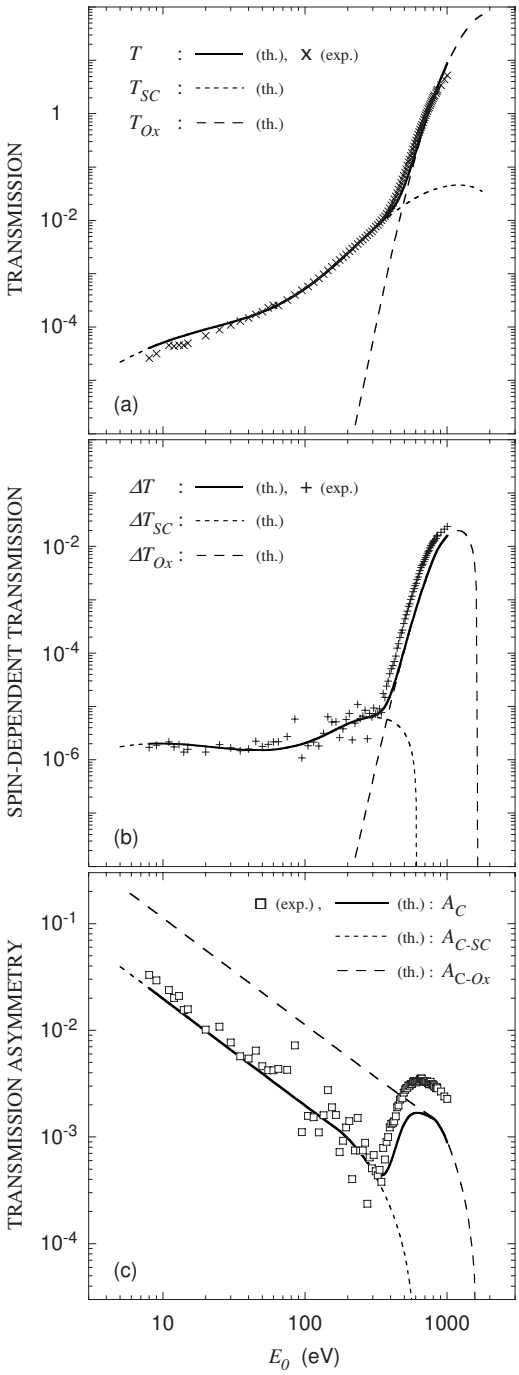

FIG. 6. (a) Calculated (full line) and experimental (symbols) variations with the injection energy E_0 of (a) the transmission T, (b) the spin-dependent transmission ΔT, (c) the transmission spin asymmetry A_C. For the three quantities T, ΔT, and A_C, the two contributions of the current transmitted above the barrier ϕ_{SC} (dotted lines) and above the barrier ϕ_{ox} (dashed lines) have been calculated.

that there is no spin relaxation along the transport. We also assume that the polarization of the secondary electrons does not depend on the incident polarization (we already mentionned that there is no significant exchange integral effect), so that we do not have to separate spin-up and spin-down secondary electron distributions. Then, for an incident beam

of spin polarization $\pm P_0$ (we take here as a convention that the incident spin polarization is positive when it is parallel to the majority spins in the ferromagnetic layer), the electron distribution $F(\varepsilon, \pm P_0)$ that forms in the metal layer and reaches the metal/oxide interface may be written as the superposition of the three distributions defined above,

$$F(\varepsilon, \pm P_0) = \frac{1 \pm P_0}{2} f_p^+(\varepsilon) + \frac{1 \mp P_0}{2} f_p^-(\varepsilon) + \left[\frac{1 \pm P_0}{2}(M^+ - 1) + \frac{1 \mp P_0}{2}(M^- - 1) \right] f_s(\varepsilon). \quad (22)$$

In this expression, $f_p^+(\varepsilon)$ and $f_p^-(\varepsilon)$ are the normalized distributions of primary electrons with spin parallel to, respectively, the majority spin and the minority spin in the magnetic metal, and $f_s(\varepsilon)$ is the normalized distribution of secondary electrons. Because of the spin asymmetry of the electron mean free path in the magnetic metal, primary electrons have a different number of collisions across the magnetic layer depending on whether their spin is parallel to the majority spins or to the minority spins. This has two consequences. The first one is that majority- and minority-spin primary electrons have different distributions $f_p^+(\varepsilon)$ and $f_p^-(\varepsilon)$: this is in fact the spin filtering effect. The second one is that majority- and minority-spin primary electrons have different secondary electron multiplication factors which are noted respectively M^+ and M^- in Eq. (22). Indeed, if we note E_p^+, E_p^-, and E_s, the respective mean energies of the three distributions $f_p^+(\varepsilon)$, $f_p^-(\varepsilon)$, and $f_s(\varepsilon)$, the total energy lost by a primary electron is $E_0 - E_p^\pm$ and this amount of energy is shared by $M^\pm - 1$ secondary electrons of mean energy E_s. Therefore, M^+ and M^- are simply given by

$$M^\pm - 1 = \frac{E_0 - E_p^\pm}{E_s}. \quad (23)$$

Note that the majority spin electrons are better transmitted than minority spin electrons, but consequently they excite less secondary electrons (M^+ is then smaller than M^-). So, the contribution of the secondary electron multiplication spin asymmetry to the spin-dependent transmission goes against that of the spin filtering effect.

Let us briefly consider the case of the injection of an unpolarized incident electron beam. We can define four useful quantities which characterize the primary electron distribution at the metal/oxide interface. First, the total primary electron distribution $f_p(\varepsilon)$ is the sum of the majority- and minority-spin primary electron contributions,

$$f_p(\varepsilon) = \frac{f_p^+(\varepsilon) + f_p^-(\varepsilon)}{2}. \quad (24)$$

Second, we note $A_p(\varepsilon)$ the spin asymmetry of $f_p(\varepsilon)$, which also represents the energy distribution of the primary electron polarization that is generated by the spin filtering effect,

$$A_p(\varepsilon) = \frac{f_p^+(\varepsilon) - f_p^-(\varepsilon)}{f_p^+(\varepsilon) + f_p^-(\varepsilon)}. \quad (25)$$

Then, we note E_p the mean energy of the primary electron distribution $f_p(\varepsilon)$,

$$E_p = \frac{E_p^+ + E_p^-}{2}, \quad (26)$$

and A_{E_p} the spin asymmetry of the primary electron mean energy,

$$A_{E_p} = \frac{E_p^+ - E_p^-}{E_p^+ + E_p^-}. \quad (27)$$

Then, using Eqs. (23)–(27) in Eq. (22), we can write $F(\varepsilon, \pm P_0)$ in a convenient form,

$$F(\varepsilon, \pm P_0) = f_p(\varepsilon) + (M-1) f_s(\varepsilon) \pm P_0 \left[A_p(\varepsilon) f_p(\varepsilon) - A_{E_p} \frac{E_p}{E_s} f_s(\varepsilon) \right], \quad (28)$$

where $M = (M^+ + M^-)/2$.

The first term $f_p(\varepsilon) + (M-1) f_s(\varepsilon)$ in Eq. (28) corresponds to the electron distribution at the junction when an unpolarized electron beam is injected into the metal layer. In the following, we will compare this term with the electron distribution $F(\varepsilon)$ as defined by Eqs. (1), (4), and (20) of the previous section: $f_p(\varepsilon) + (M-1) f_s(\varepsilon) = F(\varepsilon) = M f(\varepsilon) = (E_0/E_M)(1/E_M)\exp(-\varepsilon/E_M)$.

On another hand, our model of energy relaxation by excitation of a secondary electron cascade implies that, at a given energy ε, the ratio of the total number of electrons to the number of primary electrons is simply given by E_0/ε: this expresses that the energy E_0 of the primary electron is shared by E_0/ε electrons of energy ε.[28] Therefore, the primary electron distribution $f_p(\varepsilon)$ can be simply obtained from the expression of the overall electron distribution $F(\varepsilon)$,

$$f_p(\varepsilon) = \frac{\varepsilon}{E_0} F(\varepsilon) = \frac{\varepsilon}{E_M} \frac{1}{E_M} \exp\left(-\frac{\varepsilon}{E_M} \right). \quad (29)$$

Now, if we consider that the barrier transmission coefficient $\alpha(\varepsilon)$ does not depend on spin, the transmission $T(\pm P_0)$ for the two opposite values of the incident polarization is obtained by integration of $\alpha(\varepsilon) F(\varepsilon, \pm P_0)$ and the spin-dependent transmission $\Delta T = T(+P_0) - T(-P_0)$ is given by

$$\Delta T = 2 P_0 \int_0^\infty \alpha(\varepsilon) \left[A_p(\varepsilon) \frac{\varepsilon}{E_M} - A_{E_p} \frac{E_p}{E_s} \right] f(\varepsilon) d\varepsilon. \quad (30)$$

Note that the mean energy of the primary electron distribution $f_p(\varepsilon)$ as defined by Eq. (29) is twice the energy of the total distribution $f(\varepsilon)$: $E_p = 2E_M$. As a consequence and since M is much larger than unity in the whole explored energy range, we can take $E_p/E_s \approx 2$ in Eq. (30).

The above description of the primary electron distribution does not allow us to determine separately $f_p^+(\varepsilon)$ and $f_p^-(\varepsilon)$. Therefore, we will take an empirical approximation for $A_p(\varepsilon)$,

$$A_p(\varepsilon) \approx \frac{g^+(\varepsilon) - g^-(\varepsilon)}{g^+(\varepsilon) + g^-(\varepsilon)}, \tag{31}$$

where $g^+(\varepsilon)$ and $g^-(\varepsilon)$ are defined by

$$g^{\pm}(\varepsilon) = \frac{\varepsilon}{E_M^{\pm}} \frac{1}{E_M^{\pm}} \exp\left(-\frac{\varepsilon}{E_M^{\pm}}\right). \tag{32}$$

We calculate E_M^+ and E_M^- following the energy relaxation model of Sec. III B. For these two calculations, we use two variations of the electron mean free path with energies, respectively, $\lambda_+(\varepsilon)$ and $\lambda_-(\varepsilon)$, which are obtained from $\lambda(\varepsilon)$ by introducing the spin asymmetry of the electron mean free path deduced from Ref. 5 (for details, see Appendix B). With the values of E_M^+ and E_M^- obtained this way, we evaluate both the primary electron distribution asymmetry $A_p(\varepsilon)$ [from Eqs. (31) and (32)] and the primary electron mean energy asymmetry A_{E_p} [from Eq. (27)]. We finally obtain from Eq. (30) the variation of ΔT plotted in Fig. 6(b). This calculation, for which we have not used any other adjustable parameters, is in very good agreement with the experimental data [square symbols in Fig. 6(b)]. We have considered the same step shape for the junction collection efficiency $\alpha(\varepsilon)$ as in Sec. III A. The two calculated contributions of the electrons transmitted above the barrier ϕ_{SC} and above the barrier ϕ_{ox} are plotted separately [dotted lines in Fig. 6(b)]. As it was already demonstrated by the variation of T, the abrupt rise in ΔT above 350 eV injection energy is due to the increasing portion of electrons which may surmount the barrier ϕ_{ox} and be collected with a high efficiency α_{ox}. This is even more clearly evidenced when analyzing the variation of the transmission spin asymmetry A_C. Indeed, for a single step barrier of height ϕ and collection efficiency α above ϕ, a very simple approximated expression of A_C can be obtained,

$$A_C = \frac{\Delta T}{2T} \approx P_0 \frac{\phi}{E_0}. \tag{33}$$

We have deduced this simple approximation from the expressions of T and ΔT of Eqs. (2) and (30) and from the expressions of the energy distributions given by Eqs. (4) and (29). We have also considered that $A_p(\varepsilon) \approx 1$ and $1 - 2A_{E_p} \ll (\phi/E_M)$, which are realistic approximations when E_M is small when compared to the barrier height ϕ (see Appendix B). Equation (33) shows that the transmission spin asymmetry is mainly given by the ratio of the collection energy to the injection energy. This can be physically understood in terms of polarization dilution by the secondary electrons. Indeed, the mean energy of the transmitted electrons is $\phi + E_M \approx \phi$, so that, according to Eq. (29), the proportion of primary electrons in the transmitted current can be approximated by $f_p(\varepsilon)/F(\phi) = \phi/E_0$. The polarization seen by the spin filter is then no more the injected polarization P_0 but the diluted polarization $P_0\phi/E_0$. Therefore, at the transition between the second and the third transmission regimes which are, respectively, dominated by electrons collected above ϕ_{SC} and by electrons collected above ϕ_{ox}, the asymmetry should jump by a factor $\phi_{ox}/\phi_{SC} \approx 6$ (the higher the transmission energy, the less diluted the polarization). This value is in reasonable agreement with the factor 10 observed experimentally [Fig. 6(c)]. The discrepancy between the estimated and experimental values is probably due to the fact that we have considered that all the energy lost by the primary electrons is entirely transferred to the secondary electrons. As such, we have certainly overestimated the multiplication factor M especially at high injection energy where the energy of the hole left by the excitation of a secondary electron is not negligible.

Note that the experimental variation of A_C demonstrates the validity of Eq. (33) which is a direct consequence of Eq. (29). This strongly supports the main assumption of our model which is that the primary and secondary electron distributions have a different shape and that their ratio (i.e., the proportion of primary electrons in the overall electron distribution) at the junction depends linearly on energy like $f_p(\varepsilon)/F(\varepsilon) = \varepsilon/E_0$. Indeed, if the two distributions had the same shape, the above simple expression of A_C given by Eq. (33) would be replaced by $A_C = P_0 E_M/E_0$, and in this case, there would be no step in the variation of A_C at high injection energy. According to Eq. (33), as long as E_M remains much smaller than ϕ, the transmission spin asymmetry A_C should decrease like $1/E_0$ (ΔT is constant and T increases like $M = E_0/E_M$). This is indeed the case up to about 100 eV [see Fig. 6(c)]. However, above this injection energy, A_C starts to decrease slightly faster than $1/E_0$. This tendency is clearly observed on the experimental data in the range from 100 to 350 eV and is even more pronounced on the calculated plots of the two barrier contributions to the transmission spin asymmetry [dotted and dashed lines in Fig. 6(c)]. This pronounced decrease of the asymmetry is related to the increase in E_M [Fig. 5(a)]. When E_M reaches values comparable with the barrier height, the approximation $A_p(\varepsilon) \approx 1$ does not hold anymore over the whole integration interval above ϕ. Indeed, $A_p(\varepsilon)$ decreases toward low energy and becomes negative (see Appendix B). This tends to reduce the spin-filtering term in the expression of ΔT [Eq. (30)]. It can even be reduced to a point where the term proportional to A_{E_p}, which originates from the spin-dependent secondary electron multiplication, becomes predominant. Therefore, ΔT should decrease and could even change its sign. This is shown in Fig. 7 which represents the calculated variation of ΔT_{SC} the spin-dependent transmission for a single barrier of height $\phi = \phi_{SC}$ with a constant transfer efficiency $\alpha(\varepsilon) = \alpha_{SC}$ above ϕ. The spin-dependent transmission indeed becomes negative for injection energy of the order of 600 eV and reaches negative values which are even much larger than the usual spin filtering effect. Note that this sign reversal may only occur if the transfer efficiency $\alpha(\varepsilon)$ remains almost constant above ϕ. In the structure studied here, the oxide layer introduces a sharp increase in $\alpha(\varepsilon)$ above ϕ_{ox}, which restores the spin-filtering efficiency and masks the effect of the spin-dependent secondary electron multiplication.

IV. CONCLUSION

We have studied spin-polarized electron transport in a ferromagnetic metal/oxide/semiconductor junction as a function of the injection energy. We have observed an increase in the electron transmission and in the spin-dependent transmission

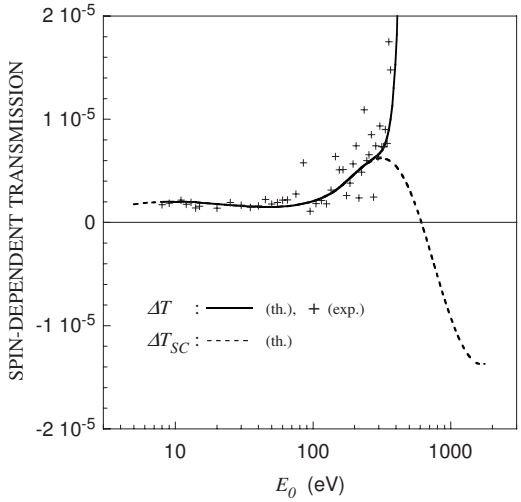

FIG. 7. Calculated variation of the spin-dependent transmission ΔT_{SC} (dashed line) versus E_0 for a single-barrier junction of height $\phi=\phi_{SC}$ and of constant transfer efficiency $\alpha=\alpha_{SC}$ above ϕ. It fits with the experimental data (symbols +) and with the full calculation of ΔT after Eq. (30) (full line) in the region where the transmitted current is dominated by electron transmitted just above ϕ_{SC}, i.e., below 300 eV injection energy. For higher injection energies, ΔT_{SC} decreases and it is predicted to become negative for injection energies larger than 600 eV.

over several orders of magnitude. The rise in the transmitted current comes from the multiplication by secondary electron excitation and from the increase in the mean energy of the electron distribution reaching the junction barrier. Since the spin-filtering effect is only related to the primary electron transmission, its stiff increase all originates from the increase in the mean energy (i.e., the width) of the transmitted electron distribution.

The increase in the mean electron energy is related to the increase in the distance crossed by electrons in the metal layer before their velocity is relaxed. Indeed, the electrons are scattered forward as long as their mean velocity is not randomized. A diffusionlike transport then takes place which favors energy relaxation. When the injection energy becomes significantly larger than the Fermi energy, the distance necessary for the relaxation of the electron velocity starts to increase. This reduces the remaining distance toward the metal/oxide interface that electrons have to cross in a three-dimensional random diffusion regime. Therefore, energy relaxation is reduced and the mean electron energy at the junction increases.

This latter effect is reinforced by the structure of the metal/oxide/semiconductor junction which exhibits two barriers of different heights and of different transfer efficiencies into the semiconductor collector: the semiconductor band-bending barrier and the oxide layer barrier. This junction structure induces a transition between two transmission regimes: at low injection energy, the current collected in the semiconductor is dominated by electrons transmitted above ϕ_{SC} after crossing the oxide layer with a poor efficiency α_{SC}, and at high injection energy, the transmission exhibits a stiff increase due to hot electrons which overcome ϕ_{ox} and are transferred into the collector with an efficiency α_{ox} of the order of unity. At the transition between these two transmission regimes, the spin-dependent component of the transmitted current also rises over almost 4 orders of magnitude, which is even more pronounced than the transmission increase. As a result, the transmission asymmetry jumps by about a factor of 10. The calculation of the spin-polarized electron transmission shows that the transmission spin asymmetry A_C is in fact mainly given by the ratio of the electron exit energy, which is determined by the barrier height ϕ, to the electron injection energy: $A_C \approx P_0 \phi / E_0$. This appears as a simple rule for the determination of the transmission spin asymmetry which may be very useful, in particular, for the design of optimized devices based on thin magnetic spin filter. In the present study, it explains that the step observed experimentally in the variation of A_C with E_0 originates from the jump in the mean electron transmission energy from ϕ_{SC} to ϕ_{ox}.

This simple rule holds as long as the exit energy of the transmitted electrons remains close to the barrier height. However, when the mean electron transmission energy becomes significantly higher than the barrier height, the spin selectivity of the junction dramatically decreases. As a consequence, the spin-filtering effect vanishes and may even be counterbalanced by the effect of the spin-dependent secondary electron multiplication. Then, the transmission spin asymmetry should become negative. Up to now, the negative transmission spin asymmetry that we predict has not been observed experimentally. It indeed requires an appropriate junction with a single barrier of moderate height and of transfer efficiency slowly varying versus energy. In the two-barrier junction studied here, this effect is not observed since it is masked by the spin-filtering effect on electrons transmitted above the oxide barrier. This is a major result for the design of devices using magnetic spin filter. Indeed, the presence of a second barrier of several eV heights and of transfer efficiency close to 1 allows us to extend the spin selectivity of the magnetic layer toward high injection energy. Indeed, over the whole probed injection energy range, the measured transmission spin asymmetry is well described with the simple approximation $A_p(\varepsilon) \approx 1$, which corresponds to spin selectivity of 100%. Therefore, high transmission (much larger than unity) and high spin-filtering efficiency (close to 100%) are obtained together when operating at high injection energy.

Moreover, not only the primary electrons are efficiently spin filtered but also the secondary electrons.[29] This has two important consequences. First, even for unpolarized injected electrons, the amplified transmitted current must be highly spin-polarized parallel to the majority spins in the ferromagnetic layer. Therefore, the electron multiplication process by the secondary electron cascade can be an efficient tool for the study of highly spin-polarized electron injection from a ferromagnetic metal into a semiconductor. Second, transistor-like devices exhibiting large magnetocurrent asymmetry together with current gain larger than unity can be envisaged when using a spin-valve structure as metallic base with a controlled base-collector barrier shape. The price to pay is to design a device whose emitter-base junction may be operated at high injection energy.

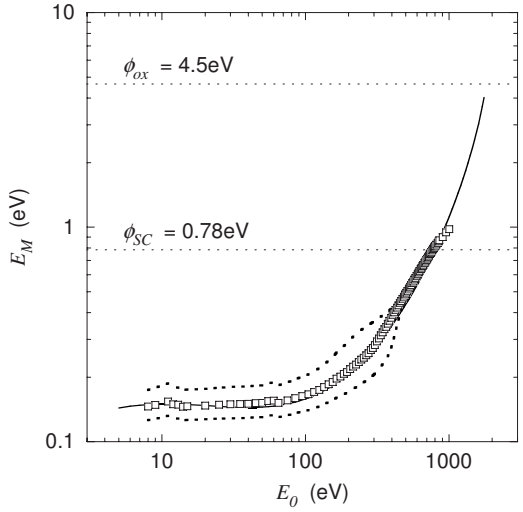

FIG. 8. Experimental (symbols) and calculated (full line) variation versus E_0 of the electron mean energy E_M at the metal/oxide interface. The experimental variation is obtained from the transmission data by solving Eq. (21) with $\alpha_{SC}=10^{-4}$ and $\alpha_{ox}=0.5$. When using $\alpha_{SC}=0.5\times10^{-4}$ or $\alpha_{SC}=2\times10^{-4}$ instead of $\alpha_{SC}=10^{-4}$ (dotted lines), the experimental variation of E_M exhibits unphysical features in the vicinity of the transition between the two transmission regimes, i.e., between 200 and 500 eV injection energies.

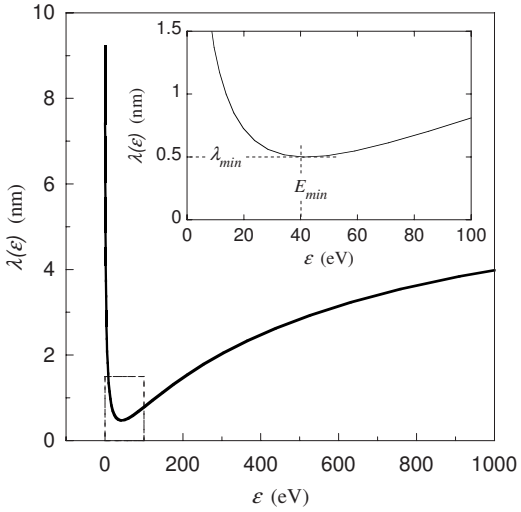

FIG. 9. Variation of the electron mean free path $\lambda(\varepsilon)$ versus energy above the Fermi level. This curve is plotted after Eq. (16) using the following set of parameters: $\lambda_l=14.5$ nm, $\lambda_h=11$ nm, $\lambda_{off}=4.8$ nm, $E_l=0.5$ eV, $E_h=1000$ eV, $a_l=0.35$, and $a_h=0.5$. The inset presents a zoom in the region of the minimum of $\lambda(\varepsilon)$. The values of $\lambda_{min}=0.5$ nm and $E_{min}=40$ eV are indicated.

ACKNOWLEDGMENTS

The authors thank D. Paget and A. Rowe for fruitful discussions and a critical reading of the paper.

APPENDIX A: VARIATION OF THE ELECTRON MEAN FREE PATH WITH ENERGY

The model developed for the calculation of the transmission involves many parameters. In order to obtain a reliable fit of the data with a reasonable number of adjustable parameters, we have used a data fitting procedure in two steps.

The first step is the determination of the variation of E_M with E_0 from the measured values of T by solving Eq. (21). This requires knowing the two barrier heights and the values of the transfer efficiency above these two barriers. For the barrier heights, we have used the measured values $\phi_{SC}=0.78$ eV and $\phi_{ox}=4.5$ eV.[24–26] For the transmission coefficients, we have taken $\alpha_{SC}=10^{-4}$ and $\alpha_{ox}=0.5$. We have first chosen arbitrarily the value of $\alpha_{ox}=0.5$ that we estimate to be reasonable because the high limit of α_{ox} is 1 and it can hardly be very much smaller than unity since the overall electron transmission reaches values much larger than unity. We have then tried different values for α_{SC} and we have found that $\alpha_{SC}=10^{-4}$ yields the most reasonable variation of E_M deduced from the transmission data (square symbols in Fig. 8). Indeed, the variation of E_M obtained with the above set of parameters is rather smooth. This is a good criterion for selecting reliable values of the transfer efficiency. Indeed, when changing the value of α_{SC} by only a factor of 2, we obtain variations of E_M which exhibit unphysical features, as shown in Fig. 8 (the dotted lines correspond to the values $\alpha_{SC}=0.5\times10^{-4}$ and $\alpha_{SC}=2\times10^{-4}$). Therefore, with this criterion, only one of the two transmission coefficients is indeed an adjustable parameter, the other one being determined by the shape of the variation of E_M with E_0.

The second step of the calculation consists in adjusting the "experimental" variation of E_M versus E_0 with the theoretical variation calculated from the model described in Sec. III B. The fit that we obtain is plotted in Fig. 8 (full line). In this calculation, we have taken $E_F=7$ eV which corresponds to the Fermi energy in palladium, and we have adjusted the variation of the electron mean free path $\lambda(\varepsilon)$. We have chosen for $\lambda(\varepsilon)$ an empirical form,

$$\lambda(\varepsilon)=\lambda_l\left(\frac{E_l}{\varepsilon+E_l}\right)^{a_l}+\lambda_h\left(\frac{\varepsilon}{\varepsilon+E_h}\right)^{a_h}-\lambda_{off}. \qquad \text{(A1)}$$

This variation, plotted in Fig. 9, reproduces the main features of the well-known universal curve.[27] The first term in Eq. (A1) gives the decrease of $\lambda(\varepsilon)$ in the low-energy range, while the second term gives the high-energy increase in $\lambda(\varepsilon)$. The third term λ_{off} is a constant that we use to control the minimum value of $\lambda(\varepsilon)$.

It is indeed known that $\lambda(\varepsilon)$ reaches a minimum value λ_{min} of the order of a few tenth of nanometers at an energy E_{min} of several tens of eV. Beyond this minimum, the increase in $\lambda(\varepsilon)$ toward high energy is approximately proportional to the square root of ε. We have taken into account these features by using three conditions which constrain the variation of $\lambda(\varepsilon)$: $a_h=0.5$, $\lambda_{min}=0.5$ nm, $E_{min}=40$ eV.

The three above conditions (which includes typical values of λ_{min} and E_{min}) allow us to reduce the number of independently adjustable parameters from seven [in Eq. (A1)] to four, which is reasonable since we are actually probing the transport properties over an energy range which goes from about 0.1 eV up to 1 keV. The fit of the variation of E_M

versus E_0 plotted in Fig. 8 (full line) has then been obtained for the following set of parameters: $\lambda_l=14.5$ nm, $\lambda_h=11$ nm, $\lambda_{off}=4.8$ nm, $E_l=0.5$ eV, $E_h=1000$ eV, $a_l=0.35$, and $a_h=0.5$. The variation of $\lambda(\varepsilon)$ corresponding to this set of parameters is the one plotted in Fig. 9.

APPENDIX B: SPIN ASYMMETRY OF THE TRANSMITTED ELECTRON DISTRIBUTION

The evaluation of the spin asymmetry of the primary electron mean energy A_{E_p} and of the primary electron distribution $A_p(\varepsilon)$, according to Eqs. (27), (31), and (32) of Sec. III D, requires the calculation of $E_M^+=E_p^+/2$ and $E_M^-=E_p^-/2$, E_p^+ and E_p^- being the mean energies of, respectively, the majority-spin and minority-spin primary electrons. For this calculation, we use basically the same procedure as for the calculation of E_M the electron mean energy at the metal/oxide interface (see Sec. III B and Appendix A), except that we take into account the spin asymmetry of the electron mean free path. We consider that spin-dependent collisions only occur during the diffusionlike transport regime (indeed, the velocity-relaxation transport step all takes place in the Pd layer, as shown in Fig. 5(b) of Sec. III B). We then calculate z_{dif}^+ and z_{dif}^- for majority-spin electrons and for minority-spin electrons by using two different variations with energy of the electron mean free path $\lambda_+(\varepsilon)$ and $\lambda_-(\varepsilon)$, respectively. Then, solving the equation $d=z_{fwd}+z_{dif}^{\pm}$ gives two different values

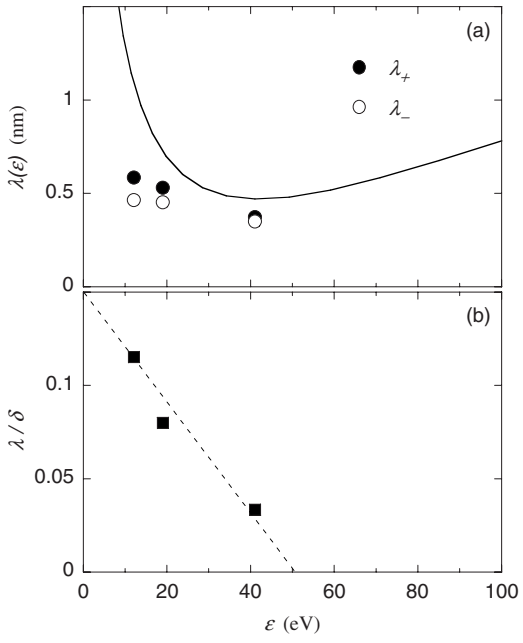

FIG. 10. (a) Variation of the electron mean free path $\lambda(\varepsilon)$ versus energy referred to the Fermi level. The full line corresponds to the variation that we have used in our calculation (see Appendix A). The symbols represent the measured values of λ_+ and λ_- taken from Ref. 5. (b) Variation of λ/δ, the spin asymmetry of the electron mean free path in iron, deduced from the above values of λ_+ and λ_- (square symbols). The dashed line corresponds to the variation of λ/δ versus ε that we have used in the expression of $\lambda_+(\varepsilon)$ and $\lambda_-(\varepsilon)$ of Eq. (B1) for the calculation of E_M^+ and E_M^-.

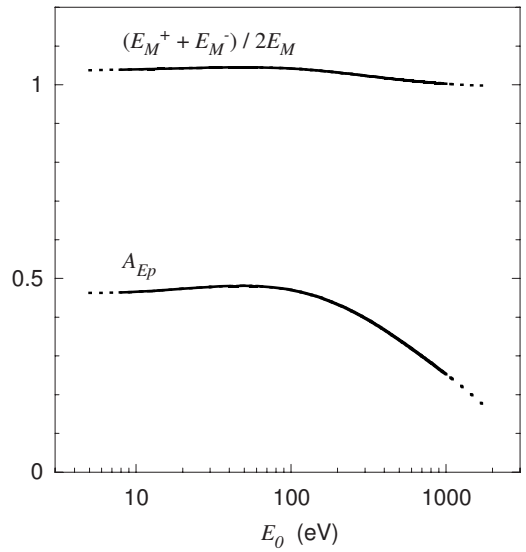

FIG. 11. Variation of $A_{E_p}=(E_M^+-E_M^-)/(E_M^++E_M^-)$, the spin asymmetry of the electron mean energy and of the ratio $(E_M^++E_M^-)/2E_M$ with injection energy E_0. These quantities are obtained from the variation of E_M, E_M^+, and E_M^-, which have been independently calculated as described in Sec. III B using, respectively, $\lambda(\varepsilon)$, $\lambda_+(\varepsilon)$, and $\lambda_-(\varepsilon)$ for the variation of the electron mean free path versus energy.

of the electron mean energy E_M^+ and E_M^-. It is important to note that E_M^+ and E_M^- are actually not the mean energies of majority- and minority-spin electrons but the mean energies of the total electron distribution if the metal was nonmagnetic and if $\lambda(\varepsilon)$ was equal to $\lambda_+(\varepsilon)$ and $\lambda_-(\varepsilon)$, respectively. The variations $\lambda_+(\varepsilon)$ and $\lambda_-(\varepsilon)$ that we have used are defined as usually by[9,10,12,14,18]

$$\frac{1}{\lambda_{\pm}(\varepsilon)} \approx \frac{1}{\lambda(\varepsilon)}\left[1 \mp \frac{\lambda(\varepsilon)}{\delta(\varepsilon)}\right], \tag{B1}$$

where $\lambda(\varepsilon)$ is the average inverse of the mean free path and $\delta(\varepsilon)$ is the so-called spin-discriminating length. The ratio $\lambda/\delta=(\lambda_+-\lambda_-)/(\lambda_++\lambda_-)$ is the spin asymmetry of the electron mean free path. From the measurements of λ_+ and λ_- reported in Ref. 5 and reproduced in Fig. 10(a), we have deduced the experimental variation of λ/δ in iron [Fig. 10(b)]. It decreases and is expected to be negligible for energies much larger than the *d*-band width. So, we have used in Eq. (B1) for the calculation of E_M^+ and E_M^- the following simple linear variation that fits with the experimental values [Fig. 10(b), dashed line]:

(i) $\lambda/\delta=0.15\ (1-\varepsilon/50)$ for $\varepsilon<50$ eV and

(ii) $\lambda/\delta=0$ for $\varepsilon>50$ eV.

Note that this variation is certainly an underestimation of λ/δ at low energy but it, however, provides a high spin selectivity.

The variations of E_M^+ and E_M^- that we obtain after this calculation verify reasonably well the relation $E_M^++E_M^-=2E_M$ (Fig. 11). These values are those used in the

calculation of ΔT which fits nicely the experimental data [see Fig. 6(b) of the main text].

A simple expression of ΔT is obtained from Eq. (30) of the main text assuming that $f_s(\varepsilon) \approx f(\varepsilon)$ and $E_s \approx E_M$,

$$\Delta T \approx 2P_0 \int_0^\infty \alpha(\varepsilon) \left[\frac{\varepsilon}{E_M} A_p(\varepsilon) - 2A_{E_p} \right] f(\varepsilon) d\varepsilon. \quad \text{(B2)}$$

The spin asymmetry of the primary electron distribution $A_p(\varepsilon)$ determines the spin-filtering effect and the spin asymmetry of the primary electron mean energy A_{E_p} determines the spin-dependent secondary electron multiplication. The variation of A_{E_p} obtained from the calculated values of E_M^+ and E_M^- is plotted in Fig. 11. Below 100 eV injection energy, A_{E_p} is almost constant and close to 0.5. Beyond 100 eV, A_{E_p} decreases very slowly: it ranges from about 0.5 to 0.25 over the entire probed energy range. Note that if minority-spin primary electrons had, in average, one more collision than majority-spin primary electrons, A_{E_p} would be equal to 2/3.

For the evaluation of $A_p(\varepsilon)$, we use Eqs. (31) and (32). Figure 12(a) shows the variation of $A_p(\varepsilon)$ for three values of the mean energy E_M: 0.15, 0.45, and 0.9 eV, which correspond to three different injection energies. The positions of the two barrier heights are indicated by vertical dotted lines. It is clear that for small values of the mean energy E_M, $A_p(\varepsilon)$ may be considered as constant and equal to unity for both contributions to the transmission, above ϕ_{SC} and above ϕ_{ox}. However, for higher values of E_M, $A_p(\varepsilon)$ cannot be taken as equal to 1 over the entire integration energy range above ϕ_{SC}. The contribution of the electron transmitted above ϕ_{SC} to the spin-dependent transmission should then tend to decrease when E_M increases. It should even become negative as it is clearly evidenced by the variation of $[(\varepsilon/E_M)A_p(\varepsilon) - 2A_{E_p}]f(\varepsilon)$ [Fig. 12(b)].

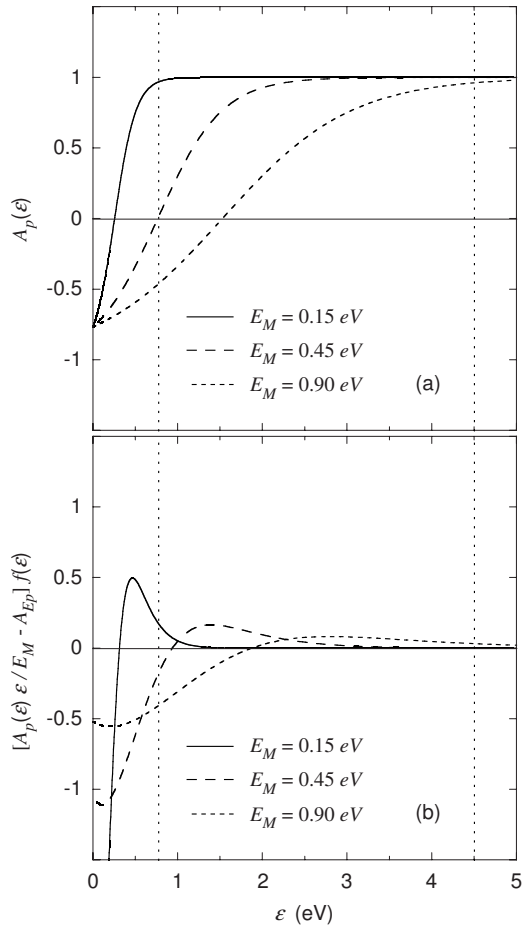

FIG. 12. Variation with electron energy of (a) $A_p(\varepsilon)$, the spin asymmetry of the electron distribution, and (b) $[A_p(\varepsilon)\frac{\varepsilon}{E_M} - 2A_{E_p}]f(\varepsilon)$. Three calculated curves are shown corresponding to three different values of the electron mean energy E_M (0.15, 0.45, and 0.9 eV) at the metal/oxide interface. The two vertical dotted lines indicate the positions of the two barrier heights ϕ_{SC} and ϕ_{ox}.

*Present address: Institut Néel, CNRS-UJF, 25 Avenue des Martyrs, B.P. 166, 38042 Grenoble Cedex 9, France.
†jacques.peretti@polytechnique.edu

[1] J. Unguris, D. T. Pierce, A. Galejs, and R. J. Celotta, Phys. Rev. Lett. **49**, 72 (1982).
[2] E. Kisker, W. Gudat, and K. Schroder, Solid State Commun. **44**, 591 (1982).
[3] H. Hopster, R. Raue, E. Kisker, G. Guntherodt, and M. Campagna, Phys. Rev. Lett. **50**, 70 (1983).
[4] D. R. Penn, S. P. Apell, and S. M. Girvin, Phys. Rev. B **32**, 7753 (1985).
[5] D. P. Pappas, K. P. Kamper, B. P. Miller, H. Hopster, D. E. Fowler, C. R. Brundle, A. C. Luntz, and Z. X. Shen, Phys. Rev. Lett. **66**, 504 (1991).
[6] M. Getzlaff, J. Bansmann, and G. Schonhense, Solid State Commun. **87**, 467 (1993).
[7] G. Schonhense and H. C. Siegmann, Ann. Phys. **2**, 465 (1993).
[8] E. Vescovo, C. Carbone, U. Alkemper, O. Rader, T. Kachel, W. Gudat, and W. Eberhardt, Phys. Rev. B **52**, 13497 (1995).
[9] Y. Lassailly, H.-J. Drouhin, A. J. van der Sluijs, G. Lampel, and C. Marliere, Phys. Rev. B **50**, 13054 (1994).
[10] A. van der Sluijs, Ph.D. thesis, Ecole Polytechnique, 1996.
[11] J. C. Grobli, D. Guarisco, S. Frank, and F. Meier, Phys. Rev. B **51**, 2945 (1995).
[12] H. J. Drouhin, A. J. vanderSluijs, Y. Lassailly, and G. Lampel, J. Appl. Phys. **79**, 4734 (1996).
[13] D. Oberli, R. Burgermeister, S. Riesen, W. Weber, and H. C. Siegmann, Phys. Rev. Lett. **81**, 4228 (1998).
[14] C. Cacho, Y. Lassailly, H. J. Drouhin, G. Lampel, and J. Peretti, Phys. Rev. Lett. **88**, 066601 (2002).
[15] D. J. Monsma, J. C. Lodder, T. J. A. Popma, and B. Dieny, Phys. Rev. Lett. **74**, 5260 (1995).
[16] T. Kinno, K. Tanaka, and K. Mizushima, Phys. Rev. B **56**, R4391 (1997).

[17] P. N. First, J. A. Bonetti, D. K. Guthrie, L. E. Harrell, and S. S. P. Parkin, J. Appl. Phys. **81**, 5533 (1997).
[18] A. Filipe, H. J. Drouhin, G. Lampel, Y. Lassailly, J. Nagle, J. Peretti, V. I. Safarov, and A. Schuhl, Phys. Rev. Lett. **80**, 2425 (1998).
[19] W. H. Rippard and R. A. Buhrman, Appl. Phys. Lett. **75**, 1001 (1999).
[20] S. van Dijken, X. Jiang, and S. S. P. Parkin, Appl. Phys. Lett. **83**, 951 (2003).
[21] X. Jiang, S. van Dijken, R. Wang, and S. S. P. Parkin, Phys. Rev. B **69**, 014413 (2004).
[22] N. Rougemaille, H.-J. Drouhin, G. Lampel, Y. Lassailly, J. Peretti, T. Wirth, and A. Schuhl, *Spin 2002: 15 International Spin Physics Symposium and Workshop on Polarized Electron Sources and Polarimeters*, AIP Conf. Proc. No. 675 (AIP, New York, 2003), p. 1001.
[23] A. Filipe and A. Schuhl, J. Appl. Phys. **81**, 4359 (1997).
[24] A. Filipe, Ph.D. thesis, Ecole Polytechnique, 1997.
[25] D. Lamine, Ph.D. thesis, Ecole Polytechnique, 2007.
[26] As discussed in Refs. 24 and 25, the oxide layer formed on GaAs is most probably Ga_2O_3. The value of the oxide band gap measured on our samples is of about 4.6 eV (see Ref. 25). This is comparable with the values between 4 and 5.2 eV that can be found in the literature for the band gap of various gallium oxides: see for instance, M. Passlak, E. F. Schubert, W. S. Hobson, M. Hong, N. Moriya, S. N. G. Chu, K. Konstadinidis, J. P. Mannaerts, M. L. Schnoes, and G. J. Zydzik, J. Appl. Phys. **77**, 686 (1995); Z. Ji, J. Du, J. Fan, and W. Wang, Opt. Mater. (Amsterdam, Neth.) **28**, 415 (2006).
[27] M. P. Seah and C. P. Hunt, Surf. Interface Anal. **5**, 33 (1983).
[28] It is sometimes considered that the primary and secondary electron distributions have identical shapes. This would only be the case if all the electrons had the same number of collisions along the transport whatever their final emerging energy (like in a thermalized electron distribution). This is not the case here and we consider that the number of collisions n that an electron undergoes during the transport across the metal layer depends on its exit energy ε. This assumption seems reasonable since, for instance, it is clear that electrons transmitted at the injection energy E_0 (i.e., with no energy loss) had no collision, while electrons transmitted with an energy very close to the barrier height have certainly suffered in average many collisions. Then, according to the energy relaxation equation that we have used [Eq. (5)], we obtain $n(\varepsilon)=\ln(E_0/\varepsilon)/\ln(2)$. Consequently, at energy ε, the ratio of the total number of electrons (primaries and secondaries together) to the number of primary electrons is $F(\varepsilon)/f_p(\varepsilon)=2^{n(\varepsilon)}=E_0/\varepsilon$.
[29] In the configuration of the present experiment, we can only measure the transmission asymmetry related to the primary electron polarization. Therefore, the polarization of the secondary electrons cannot be evidenced since its orientation is determined by that of the magnetic layer magnetization and not by the primary electron polarization. To evidence the spin filtering of secondary electrons, one should either use a spin-valve structure or measure the polarization of the transmitted electrons.